高温高压下 CL-20 的晶格参数和力学性能理论模拟

谭嘉进[1,2]，李小燕[3]，于白茹[4]，李　洋[1]，李艳芳[1]，葛妮娜[2]，袁姣楠[2]，姬广富[2]
(1. 东华理工大学理学院，南昌 330013；2. 中国工程物理研究院流体物理研究所，绵阳 621900；
3. 东华理工大学核科学与工程学院，南昌 330013；4. 四川大学物理学院，成都 610064)

摘　要：利用分子动力学结合 COMPASS 力场方法研究高能含能材料六硝基六氮杂异伍兹烷. 模拟室温下 ε 晶相 CL-20 在 0～10 GPa 压强区间，α 晶相、β 晶相和γ晶相 CL-20 在 0～20 GPa 压强区间的晶格参数和弹性常数. 同时还模拟了室压下 CL-20 在 100～500 K 温度区间的晶格参数和弹性常数. 对于自然状态下最稳定的 ε 晶相 CL-20，我们模拟得到的晶格常数、晶胞体积-压强关系和弹性常数理论结果和实验数据非常吻合. 所以对其它晶相 CL-20 模拟结果的准确性提供了佐证. 理论预测 CL-20 在不同温度和压强下的晶格常数和力学性能对于工程应用具有积极的指导意义.

关键词：分子动力学；含能材料；晶格参数；弹性常数
中图分类号：O56　　**文献标识码**：A　　DOI：10.19907/j.0490-6756.2021.014003

Theoretical predictions of lattice parameters and mechanical properties of CL-20 under the temperature and pressure

TAN Jia-Jin[1,2], *LI Xiao-Yan*[3], *YU Bai-Ru*[4], *LI Yang*[1],
LI Yan-Fang[1], *GE Ni-Na*[2], *YUAN Jiao-Nan*[2], *JI Guang-Fu*[2]
(1. College of Science, East China University of Technology, Nanchang 330013, China;
2. Institute of Fluid Physics, Chinese Academy of Engineering Physics, Mianyang 621900, China;
3. College of Nuclear Science and Engineering, East China University of Technology, Nanchang 330013, China;
4. College of Physics, Sichuan University, Chengdu 610064, China)

Abstract: The molecular dynamics with condensed-phase optimized molecular potentials for atomistic simulation studies (COMPASS) force field have been employed to study high energetic material CL-20. The lattice parameters and elastic constants in the pressure range of 0～10 GPa (for ε-CL-20) and 0～20 GPa (for α-, β-, and γ-CL-20) at room temperature, and in the temperature range of 100～500 K at room pressure are predicted. The good agreement of lattice parameters, pressure-volume relation and elastic constants of the greatest stability phase ε-CL-20 shows the accuracy of our simulations. The theoretical predictions of lattice parameters and mechanical properties of CL-20 under temperature and pressure may provide powerful guidelines for the engineering application and await further experimental confirmation.

Keywords: Molecular dynamics; Energetic materials; Lattice parameter; Elastic constants

收稿日期：2020-11-13
基金项目：国家自然科学基金(11664002，41761090)；中国博士后科学基金(2014M562336)
作者简介：谭嘉进(1983－)，男，山东青岛人，副教授，主要研究含能材料物性模拟. E-mail：tjjscu@126.com
通讯作者：于白茹. yubrscu@126.com

1 Introduction

2,4,6,8,10,12-hexanitro -2,4,6,8,10,12-hexaazaisowurtzitane (CL-20) has the largest density in the current existing energetic materials, and it is superior to conventional high-energy propellants and explosives[1-2]. Thus, CL-20 is considered as the most potential and powerful high energy density materials. Its synthesis has been a breakthrough in the synthesis of high explosive investigations. CL-20 is a caged nitramine explosive with the formula $C_6H_6N_{12}O_{12}$, as shown in Fig. 1. The structure of CL-20 molecule consists of two five-member rings and a six-member ring. There exhibits four different crystal structures of CL-20, three pure crystallization phases, β, γ, and ε, and a hydrate phase α at ambient conditions, as shown in Fig. 2.

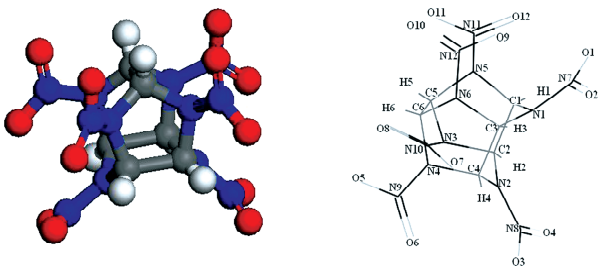

Fig. 1　Conformation and atomic numbering of $C_6H_6N_{12}O_{12}$ molecule in CL-20

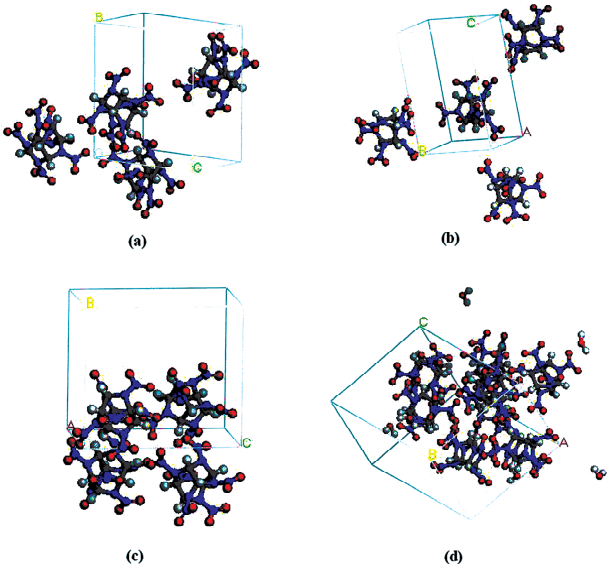

Fig. 2　Unit cell of CL-20: (a) ε- CL-20, (b) γ- CL-20, (c) β- CL-20 and (d) α- CL-20

At ambient conditions, the stabilities of these polymorphs are known to be ε>γ>α>β. ε-CL-20 has the largest density and best thermochemical stability among them, which makes it the popular phase for applications and investigation. Up to now, several experimental[3-4] and theoretical[5-7] studies have been reported for ε-CL-20. In experimental studies, Pinkerton has reported the pressure-volume relationship of this polymorph up to 2.5 GPa firstly[3]. Later, Gump and Peiris have measured the isothermal compression data of ε-CL-20 up to 5.6 GPa both at ambient temperature and 75 ℃[4]. The ambient-temperature isothermal bulk modulus of 13.6 GPa with a pressure derivative of 11.7 has also been reported according to the third-order Birch-Murnaghan equation of state (EOS)[4]. In theoretical studies, some efforts have been done to investigate the EOS of CL-20 through density functional theory (DFT)[5-6], Molecular dynamics (MD) simulation[7], and molecular packing (MP) method[7], respectively. Based on DFT, using GGA-PW91 method, the ultrasoft pseudopotentials (USP) with 396 and 545 eV planewave basis set have been employed to calculate the EOS of ε-CL-20, respectively[5]. Compared with the 396 eV predictions, the 545 eV predictions show larger deviations from the experiment, especially in the low range of pressure. It should be noted that the agreement of 396 eV results origin from the insufficiency of energy cutoff for the plane-wave basis set. Subsequently, Sorescu and Rice calculated the lattice parameters of CL-20 under pressure using DFT method with a plane-wave basis set of within the pseudopotential approximation[6]. The calculated pressure-volume relationship of CL-20 also has large deviations from the corresponding experimental data, as the similarity as of 545 eV results[6]. The large deviations in both the lattice parameters and EOS for energetic materials CL-20 are mainly due to a lacking reproduce of van der Waals (vdW) forces in current DFT. In addition, both of the MD within the rigid-molecule approximation and MP methods are employed to calculate

the pressure - volume relation of CL-20[7]. The calculated zero pressure lattice parameters are accurate, but the deviations have been getting larger with increasing pressure for comparison with the experimental results. These results indicate that both of the two methods can not predict the accurate lattice parameters under high pressure[7]. The condensed-phase optimized molecular potentials for atomistic simulation studies (COMPASS) force field could give the well description of the intermolecular interaction potential. As this theory could effectively improve the accuracy of the simulations for energetic materials, it has been employed for simulating the energetic materials, such as HMX[8] and RDX[9]. In this paper, we also employ the MD simulations with COMPASS force field to investigate the lattice dynamics of CL-20.

At present, CL-20 has not been fielded in military and civil applications yet because of its high sensitivity. Some efforts have been done to reduce the mechanical sensitivities of CL-20 based polymer bonded explosives such that the hazardous energetic material may be handled and even machined into desired shapes[10-13]. Whatever, it is fundamental and significant to know the mechanical properties of pure CL-20 from atomic and molecular scale. As is well known, the elastic constant is a key parameter to investigate the mechanism properties. Though the experimental approaches of elastic constants, such as Brillouin scattering, ultrasonic velocity measurements, and resonant ultrasound spectroscopy, are mature technology, it is still difficult to measure the elastic constants of energetic materials accurately. For example, HMX(C_{22}, C_{33}, C_{55}, C_{66}, C_{23})[14-16] and RDX(C_{11}, C_{22}, C_{44}, C_{12})[17-19], the experimental data differ from each other and some deviations are very large. This is because that the samples of energetic materials are not perfect enough with some crystallographic defects. In literature, only one experimental study on the elastic constants of ε-CL-20 has been reported by Haycraft using Brillouin scattering spectroscopy at ambient conditions[20]. The theoretical investigation on the elastic properties of the other phase (α-, β-, and γ-CL-20) are lacking in literature, especially in high pressure and temperature range.

The goal of this work is to predict the lattice parameters and mechanical properties under high temperature and pressure of four CL-20 crystal phases (α-, β-, γ-, and ε-CL-20). This work is respected to give a comparative and complementary theoretical support for experiments.

2 Computational details

2.1 Molecular dynamics calculations

The MD simulations with COMPASS[21] force field are employed for four polymorphs (α-, β-, γ-, and ε-CL-20). The initial lattice parameters and internal atomic coordinates are taken from experimental data. ε- and γ-CL-20 belong to the monoclinic symmetry, while α- and β-CL-20 belong to the orthorhombic symmetry. The conformation and atomic numbering of $C_6H_6N_{12}O_{12}$ molecule are shown in Fig. 1, together with the unit cell of four pure polymorphs, which are plotted in Fig. 2. The molecular dynamics simulations are performed with the Discover code. A computational supercell size of 2×2×2 unit cells are done. The MD simulations are carried out in the isothermal - isobaric NPT ensemble with the Andersen thermostat method[22] and Berendsen barostat method[23] to control the system pressures and temperatures respectively. The long-range non-bond Coulombic and vdW interactions are managed using the Ewald simulation method[24]. The calculated system is relaxed for 1×10^5 time steps with the time step of 1 fs in the equilibration run at each target of temperature and pressure.

2.2 Elastic constants

The elastic stiffness tensor c_{ijkl} can be expressed as

$$\sigma_{ij} = \sum_{kl}^{1,3} c_{ijkl}\varepsilon_{kl} \tag{1}$$

where ε_{kl} is the strain, c_{ijkl} is the elastic constant (matrix) and σ_{ij} is the stress. There are thirteen

independent components of the elastic stiffness tensor for monoclinic crystal, and nine independent components for orthorhombic crystal.

For monoclinic phase[25]

$$B_V=(1/9)[C_{11}+C_{22}+C_{33}+2(C_{12}+C_{13}+C_{23})] \quad (2)$$

$$G_V=(1/15)[C_{11}+C_{22}+C_{33}+3(C_{44}+C_{55}+C_{66})]-(C_{12}+C_{13}+C_{23}), \quad (3)$$

$$B_R=h[a(C_{11}+C_{22}-2C_{12})+b(2C_{12}-2C_{11}-C_{23})+c(C_{15}-2C_{25})+c(C_{15}-2C_{25})+d(2C_{12}+2C_{23}-C_{13}-2C_{22})+2e(C_{25}-C_{15})+f]^{-1} \quad (4)$$

$$G_R=15\{4[a(C_{11}+C_{22}+C_{12})+b(C_{11}-C_{12}-C_{23})+c(C_{15}+C_{25})+d(C_{22}-C_{12}-C_{23}-C_{13})+e(C_{15}-C_{25})+f]/h+3[g/h+(C_{44}+C_{66})/(C_{44}C_{66}-C_{46}^2)]\}^{-1} \quad (5)$$

$$a=C_{33}C_{55}-C_{35}^2$$

$$b=C_{23}C_{55}-C_{25}C_{35}$$

$$c=C_{13}C_{35}-C_{15}C_{33}$$

$$d=C_{13}C_{55}-C_{15}C_{35}$$

$$e=C_{13}C_{25}-C_{15}C_{23}$$

$$f=C_{11}(C_{22}C_{55}-C_{25}^2)-C_{12}(C_{12}C_{55}-C_{15}C_{25})+C_{15}(C_{12}C_{25}-C_{15}C_{22})+C_{25}(C_{23}C_{35}-C_{25}C_{33})$$

$$g=C_{11}C_{22}C_{33}-C_{11}C_{23}^2-C_{22}C_{13}^2-C_{33}C_{12}^2+2C_{12}C_{13}C_{23}$$

$$h=2[C_{15}C_{25}(C_{33}C_{12}-C_{13}C_{23})+C_{15}C_{35}(C_{22}C_{13}-C_{12}C_{23})+C_{25}C_{35}(C_{11}C_{23}-C_{12}C_{13})]-[C_{15}^2(C_{22}C_{33}-C_{23}^2)+C_{25}^2(C_{11}C_{33}-C_{13}^2)+C_{35}^2(C_{11}C_{22}-C_{12}^2)]+gC_{55}$$

For orthorhombic phase[26]

$$B_V=(1/9)[C_{11}+C_{12}+C_{33}+2(C_{12}+C_{13}+C_{23}) \quad (6)$$

$$G_V=(1/15)[C_{11}+C_{22}+C_{33}+3(C_{44}+C_{55}+C_{66})-(C_{12}+C_{13}+C_{23}) \quad (7)$$

$$B_R=\Delta[C_{11}(C_{22}+C_{33}-2C_{23})+C_{22}(C_{33}-2C_{13})-2C_{33}C_{12}]+C_{12}(2C_{23}-C_{12})+C_{13}(2C_{12}-C_{13})+C_{23}(2C_{13}-C_{23})]^{-1} \quad (8)$$

$$G_R=15\{4[C_{11}(C_{22}+C_{33}+C_{23})+C_{22}(C_{33}+C_{13})+C_{33}C_{12}\}-C_{12}(2C_{23}+C_{12})-C_{13}(2C_{12}+C_{13})-C_{23}(C_{13}+C_{23})]/\Delta+3[(1/C_{44})+(1/C_{55})+(1/C_{66})]\}^{-1} \quad (9)$$

$$\Delta=C_{13}(C_{12}C_{23}-C_{13}C_{22})+C_{23}(C_{12}C_{13}-C_{23}C_{11})+C_{33}(C_{11}C_{22}-C_{12}^2)$$

The arithmetic average of the Voigt and Reuss bounds is named the Voigt-Reuss-Hill (VRH) average and employed to estimate the elastic moduli of polycrystals[27-29]:

$$B_V+B_R=2B_H,\ G_V+G_R=2G_H \quad (10)$$

Young's modulus E can be calculated by

$$E=9BG/(3B+G) \quad (11)$$

Possion's ratio ν are obtained by the following formula

$$\nu=(3B-2G)/[2(3B+G)] \quad (12)$$

3 Results and discussion

3.1 Lattice parameters

The calculated lattice constants and unit cell volume at ambient conditions from our NPT-MD optimizations are shown in Tab. 1, together with the available experimental[30-31] and other theoretical data[6-7]. With regard to experiments, the deviation of our calculated unit cell volume are −0.46% (ε-CL-20), −3.48% (γ-CL-20), 2.02% (α-CL-20), and −1.61% (β-CL-20). Our calculated results agree with the experimental and theoretical results.

Tab. 1 Calculated equilibrium lattice parameters at ambient conditions in comparison to the theoretical and experimental values

Phase	Data source	Method	a_0/Å	b_0/Å	c_0/Å	v_0/Å^3	error (v_0)
ε	This work	NPT-MD	8.849	12.574	13.374	1 423.67	−0.46%
	Ref. [6]	DFT-D	8.916	12.514	13.413	1 434.43	0.29%
	Ref. [7]	NPT-MD	8.895 6	12.577 4	13.548 1	1 461.607 6	2.19%
	Ref. [30]	Expt.	8.862 8	12.592 8	13.394 7	1 430.24	—
γ	This work	NPT-MD	13.072	8.073	14.717	1 467.02	−3.48%

(**Tab.** 1　**Continued**)

Phase	Data source	Method	a_0/Å	b_0/Å	c_0/Å	v_0/Å^3	error (v_0)
	Ref. [6]	DFT-D	13.214	8.223	14.764	1 518.58	−0.09%
	Ref. [30]	Expt.	13.227 2	8.169 2	14.892	1 519.99	—
α	This work	NPT-MD	9.610	13.320	23.792	3 045.50	2.02%
	Ref. [31]	Expt.	9.546	13.232	23.634	2 985.27	—
β	This work	NPT-MD	9.641	11.578	12.920	1 442.18	−1.61%
	Ref. [6]	DFT-D	9.659	11.485	13.251	1 469.96	0.29%
	Ref. [31]	Expt.	9.693	11.641	12.990	1 465.74	—

3.2　Equation of state

The EOS is important for mitigation of hazardous materials like CL-20 in preparation, transportation, storage, and handing process. We plot the variation of lattice parameters under pressure or temperature in Fig. 3.

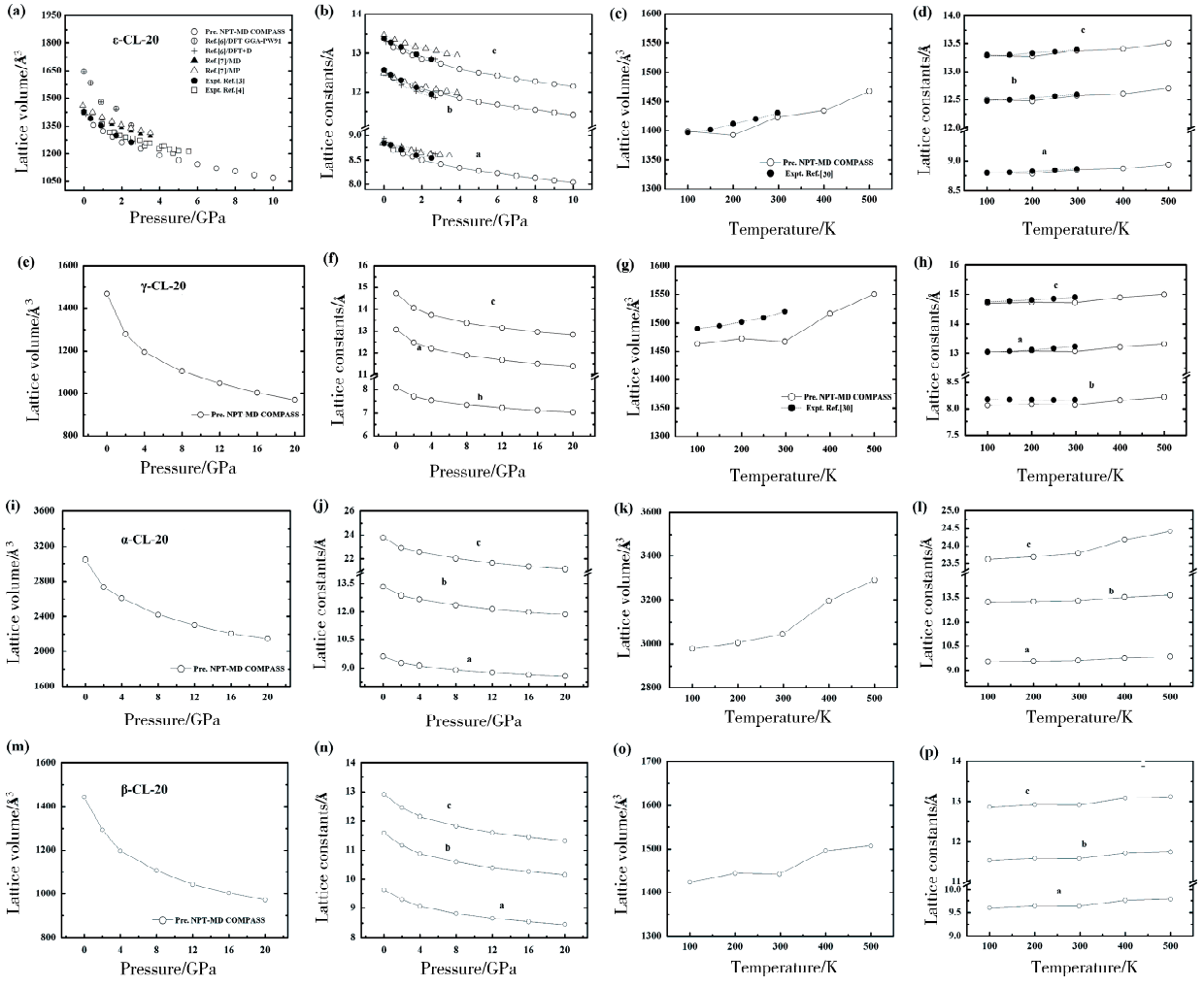

Fig. 3　Variation of cell volume and lattice constants of ε-CL-20 (a～d), γ-CL-20 (e～h), α-CL-20 (i～l), β-CL-20 (m～p) with pressure at 298 K, or with temperature at room pressure

As shown in Fig. 3(a), for the ε-CL-20, the zero pressure theoretical crystal volume with DFT method overshoot the experimental results[3-4] and then the discrepancy gets smaller with increasing pressure. Due to the poor description of vdW force, which plays an important role in CL-20 molecular crystal, the DFT calculation overestimates the cell volume[7]. While the dispersion-corrected simulations using a semi-empirical correction term proportional added to Kohn-Sham

energy functional improve the accuracy[7]. The zero pressure theoretical crystal volumes from the MP and NPT-MD method agree well with the experimental results, while the discrepancy increases with increasing pressure. These results suggest that the intermolecular potential used in the MP and NPT-MD methods can not predict lattice parameters accurately under high pressure[14]. Our calculated results of NPT-MD method with CMPASS force field agree well with experimental data[3-4]. Similarly, our theoretical predictions of lattice parameters consist well with the experiments in the temperature range of 100 to 298 K[30]. Though the experimental data for comparison is insufficient, our theoretical predictions of lattice parameters should be accurate in the higher pressure or temperature range. In addition, we predict the lattice parameters of α-CL-20, β-CL-20, and γ-CL-20 in the pressure range of 0 to 20 GPa or in the temperature range of 100 to 500 K, as is shown in Fig. 3(e) ~ 3(p).

There are several different formulations of EOS. Here, we fit the *P-V* data of CL-20 to Murnaghan EOS[32] and Birch-Murnaghan EOS[33] respectively. The third-order Birch-Murnaghan EOS can be written as follows,

$$P=3B_0 f_E (1+2f_E)^{\frac{5}{2}}(1+3/2(B_0'-4)f_E) \tag{13}$$

where f_E is written as $f_E=[(V_0/V)^{\frac{2}{3}}-1]/2$. The Murnaghan EOS is written in the form of

$$P=B_0/B_0'[(V_0/V)^{B_0'}-1] \tag{14}$$

Fitting the *P-V* data to the EOS yields the bulk modulus and its first pressure derivative of CL-20, which are listed in Tab. 2, together with the experimental[4] and theoretical data[7]. The calculated B_0 and B_0' of ε-CL-20 obtained through the fit to Birch-Murnaghan EOS show good agreement with the experimental values. Because our predicted pressure-volume points approach experiments well, especially in the low pressure range[3-4], as can be found in Fig. 1(a). The accuracy of the calculated B_0 and B_0' of α-, β-, and γ-CL-20 still await the experimental confirmation.

Tab. 2　The calculated bulk modulus B_0 and its first pressure derivative B_0' of CL-20 compared with experimental and theoretical values

Phase	Data source	Method	EOS	B_0/GPa	B_0'
ε	This work	NPT-MD	BM	9.9	10.2
	This work	NPT-MD	M	11.8	6.6
	Ref. [7]	NPT-MD	M	15.58	9.37
	Ref. [4]	Expt.	BM	13.6±2.0	11.7±3.2
γ	This work	NPT-MD	BM	5.9	14.7
	This work	NPT-MD	M	9.8	6.4
α	This work	NPT-MD	BM	11.4	11.3
		NPT-MD	M	15.0	6.4
β	This work	NPT-MD	BM	8.5	11.4
		NPT-MD	M	11.6	6.2

BM: Birch-Murnaghan equation of state;
M: Murnaghan equation of state

3.3 Elastic and mechanical properties

Though the experimental approaches of elastic constants, such as Brillouin scattering, ultrasonic velocity measurements, and resonant ultrasound spectroscopy (RUS), are mature technology, it is still difficult to measure the elastic constants of energetic materials accurately. Several experimental efforts have been done on the conventional explosives, RDX and HMX. The experimental data differ from each other and some deviations are large, such as HMX (C_{22}, C_{33}, C_{55}, C_{66}, C_{23})[14-16] and RDX (C_{11}, C_{22}, C_{44}, C_{12})[17-19]. Due to the poor description of vdW force, which plays an important role in CL-20 molecular crystal, the DFT calculation can not predict the elastic constants of CL-20 accurately. The good predictions of lattice parameters and EOS above indicate that the molecular dynamics simulations with COMPASS force field can give accurate description of interatomic binding forces and intermolecular interaction in CL-20 crystal. The elastic constants of four polymorphs at ambient conditions (α-, β-, γ-CL-20, and ε-CL-20) are listed in Tab. 3. The good agreement of experimental and theoretical elastic constants for ε-CL-20 proves the validity and accuracy of the calculation for CL-20. The elastic modulus of CL-20 under temperature at room pressure or under pres-

sure at 298 K are calculated and listed in Tab. 4. The temperature and pressure are the influencing factors in preparation, transportation, storage, and handing process. The predicted elasticity under temperature and pressure can provide powerful guidelines for the engineering application and further experimental investigations.

We plot the variation of bulk modulus B, shear modulus G, Young's modulus E, and Possion's ratio ν as a function of the pressure as shown in Fig. 4. The mechanical moduli of α-, β-, γ-, and ε-CL-20 are found to increase with increasing pressure. On account of the greatest stability of ε phase among the four polymorphs, we also calculate the temperature dependence of bulk modulus B, shear modulus G, Young's modulus E, and Possion's ratio ν for ε-CL-20, as listed in Tab. 5. Though there are no experimental mechanical moduli at different temperature for comparison, the good agreement of bulk modulus B_H and shear modulus G_H at ambient conditions shows the accuracy of our simulations[20]. The mechanical moduli under temperature can be fitted to a third order polynomial, *i.e.*,

Tab. 3　The calculated C_{ij} of CL-20 at ambient conditions and the experimental data for ε-CL-20

C_{ij}/GPa	ε-CL-20		γ-CL-20	α-CL-20	β-CL-20
	This work	Expt.[20]	This work	This work	This work
C_{11}	17.81	7.70	13.47	8.66	7.41
C_{22}	18.25	28.29	13.93	6.97	13.99
C_{33}	30.95	28.05	13.72	13.79	5.47
C_{44}	8.26	12.64	5.57	2.65	8.14
C_{55}	4.10	3.86	2.61	7.51	3.23
C_{66}	3.55	4.73	2.11	3.56	1.86
C_{12}	6.92	5.69	6.91	2.09	8.86
C_{13}	4.55	9.21	5.30	7.29	3.26
C_{23}	1.22	−1.22	4.74	4.92	2.52
C_{15}	1.52	1.23	−0.26		
C_{25}	1.62	1.01	−2.43		
C_{35}	0.00	3.07	−0.75		
C_{46}	−0.61	0.74	−0.06		

Tab. 4　The calculated elastic modulus C_{ij} of CL-20 under temperature at room pressure or under pressure at 298 K

		C_{ij} / GPa												
		C_{11}	C_{22}	C_{33}	C_{44}	C_{55}	C_{66}	C_{12}	C_{13}	C_{23}	C_{15}	C_{25}	C_{35}	C_{46}
ε-CL-20	T/K													
	100	23.33	21.70	36.20	9.97	4.62	4.03	9.02	6.18	1.48	2.00	2.14	0.25	−0.78
	200	20.60	20.02	33.75	9.16	4.38	3.79	7.98	5.37	1.39	1.76	1.89	0.12	−0.70
	298	17.81	18.25	30.95	8.26	4.10	3.55	6.92	4.55	1.22	1.52	1.62	0.00	−0.61
	400	14.71	16.15	27.43	7.20	3.77	3.27	5.72	3.68	0.96	1.29	1.33	−0.08	−0.46
	500	11.37	12.72	23.45	6.00	3.19	2.96	4.47	2.66	0.85	0.98	0.93	0.08	−0.28
	P/GPa													
	10^{-4}	17.81	18.25	30.95	8.26	4.10	3.55	6.92	4.55	1.22	1.52	1.62	0.00	−0.61
	2	49.13	37.50	53.55	16.23	6.61	6.28	20.22	15.80	3.11	4.99	4.44	1.99	−1.10
	4	72.69	49.83	67.86	20.56	8.61	8.66	32.31	27.61	6.47	8.24	6.11	2.69	−1.53
	6	92.27	55.92	80.67	22.45	10.20	11.23	42.83	38.06	11.56	10.50	5.82	0.93	−2.49
	8	26.10	58.14	99.44	20.45	3.16	13.88	36.46	45.37	27.61	−17.67	−0.20	−4.45	−3.42
	10	54.80	70.39	115.60	21.50	13.31	14.49	45.60	51.07	37.66	−11.71	2.27	−9.95	1.44
γ-CL-20	T/K													
	100	18.02	18.96	11.93	7.52	2.75	2.70	8.38	7.45	7.43	−1.15	−3.25	2.71	−1.45
	200	15.16	14.99	16.10	3.64	2.20	2.82	7.33	5.80	5.12	−0.63	−2.36	−1.47	0.66
	298	13.47	13.93	13.72	5.57	2.61	2.11	6.91	5.30	4.74	−0.26	−2.43	−0.75	−0.06
	400	11.64	7.75	9.45	5.25	0.57	1.96	5.09	3.66	3.70	0.04	−2.74	−3.45	0.22
	500	10.13	9.63	8.39	4.01	1.49	1.69	4.98	2.91	2.97	−0.47	−1.99	−0.25	0.67
	P/GPa													
	10^{-4}	13.47	13.93	13.72	5.57	2.61	2.11	6.91	5.30	4.74	−0.26	−2.43	−0.75	−0.06

(**Tab.** 4　**Continued**)

		C_{ij} / GPa												
		C_{11}	C_{22}	C_{33}	C_{44}	C_{55}	C_{66}	C_{12}	C_{13}	C_{23}	C_{15}	C_{25}	C_{35}	C_{46}
	4	50.69	50.56	49.92	16.52	8.31	12.48	26.10	23.66	32.87	2.24	−7.27	−2.25	−3.78
	8	81.94	73.26	75.88	24.29	10.46	15.29	46.66	41.95	46.93	4.30	−4.62	−3.37	−2.90
	12	97.58	95.92	101.40	26.64	14.29	17.54	63.77	61.96	59.28	2.47	−1.27	−2.97	−2.35
	16	120.10	120.90	132.30	28.82	18.12	15.47	85.64	81.06	72.26	4.06	−0.99	−1.65	−4.26
	20	147.50	154.00	153.00	31.59	22.70	20.87	98.64	95.50	87.28	5.55	−2.01	−3.93	1.99
α-CL-20	T/K													
	100	12.15	8.66	20.95	4.24	8.97	4.50	3.45	14.37	11.42				
	200	11.81	8.60	18.43	3.59	8.66	5.29	3.39	10.66	6.92				
	298	8.66	6.97	13.79	2.65	7.51	3.56	2.09	7.29	4.92				
	400	9.62	7.21	10.37	2.26	4.59	2.98	4.73	3.90	3.02				
	500	4.67	4.30	7.32	1.38	2.42	2.56	2.74	2.68	1.48				
	P/GPa													
	10^{-4}	8.66	6.97	13.79	2.65	7.51	3.56	2.09	7.29	4.92				
	4	44.99	48.64	58.54	14.59	19.69	13.28	21.31	31.45	25.05				
	8	72.53	76.99	97.28	19.01	25.26	17.00	38.78	59.56	38.37				
	12	95.48	102.00	106.40	24.12	26.97	20.24	57.46	70.18	60.22				
	16	122.10	123.40	132.80	28.06	30.70	27.76	73.94	83.91	78.61				
	20	122.10	146.40	153.40	28.87	34.77	28.60	92.70	98.09	94.38				
β-CL-20	T/K													
	100	11.04	25.85	0.31	15.63	4.94	2.55	13.49	8.20	8.43				
	200	10.09	23.86	−0.87	14.42	4.49	2.52	12.34	6.32	7.17				
	298	7.41	13.99	5.47	8.14	3.23	1.86	8.86	3.26	2.52				
	400	7.26	14.78	6.69	6.44	3.62	2.19	8.82	4.24	3.34				
	500	5.94	11.26	5.73	5.73	2.64	1.72	7.52	5.50	4.86				
	P/GPa													
	10^{-4}	7.41	13.99	5.47	8.14	3.23	1.86	8.86	3.26	2.52				
	4	40.77	33.95	51.93	6.22	16.72	11.37	31.84	26.37	27.10				
	8	66.76	60.20	81.49	18.46	23.97	18.65	51.13	43.61	44.97				
	12	92.13	93.50	104.90	27.48	27.77	19.02	71.77	60.97	60.10				
	16	109.70	126.70	132.80	31.06	29.67	23.61	83.05	79.15	78.54				
	20	148.60	147.40	145.20	30.56	34.52	19.66	104.10	93.31	92.03				

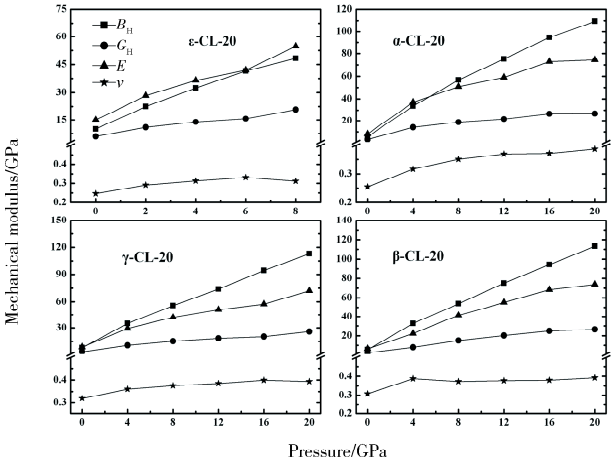

Fig. 4　The calculated pressure dependence of bulk modulus B_H (squares), shear modulus G_H (circles), Young's modulus E (triangles), and Possion's ratio ν (stars) for CL-20

Tab. 5　The calculated temperature dependence of bulk modulus B, shear modulus G, Young's modulus E, and Possion's ratio ν for ε-CL-20

T/K	B_V /GPa	B_R /GPa	B_H /GPa	G_V /GPa	G_R /GPa	G_H /GPa	E /GPa	ν
100	12.73	11.87	12.30	8.03	6.20	7.12	17.89	0.258
200	11.54	10.82	11.18	7.44	5.80	6.62	16.59	0.253
298	10.27	9.67	9.97	6.80	5.36	6.08	15.17	0.246
298	10.16[a]	7.15[a]	8.65[a]	7.60[a]	3.76[a]	5.68[a]		
400	8.78	8.28	8.53	6.04	4.84	5.44	13.47	0.237
500	7.05	6.58	6.82	5.07	4.12	4.60	11.25	0.225

[a]The data in Ref. [20] is calculated on the basis of the ambient experimental elastic constants by the Voigt-Reuss-Hill approximation.

$$B_H(T) = 13.411 - 0.011T + 3.823 \times$$

$$10^{-6}\ T^2-1.502\times10^{-8}T^3 \quad (15)$$

$$G_H(T)=7.682-0.006T+6.633\times 10^{-6}\ T^2-1.338\times10^{-8}T^3 \quad (16)$$

$$E(T)=19.320-0.015\ T\ +1.539\times 10^{-5}\ T^2-3.344\times10^{-8}T^3 \quad (17)$$

$$\nu(T)=0.262-3.463\times10^{-5}T\ -3.632\times 10^{-8}T^2-8.412\times10^{-11}T^3 \quad (18)$$

4 Conclusions

Molecular dynamics simulations have been employed to study the lattice parameters, EOS, elastic constants, and mechanical modulus under pressure and temperature. The good agreement between molecular dynamics results and experimental data prove that the molecular dynamics simulations with COMPASS force field can give good description of interatomic binding forces and intermolecular interaction in CL-20 crystal. From the above investigations, we have the following conclusions:

(1) The calculated equilibrium lattice parameters of four polymorphs (α-, β-, γ-, and ε-CL-20) at ambient conditions are in good agreement with the experiments. We predict the lattice parameters of CL-20 under pressure and temperature. The bulk modulus B_0 and its pressure derivative B_0' are obtained by fitting the pressure-volume points to Birch-Murnaghan EOS and Murnaghan EOS respectively.

(2) The elastic constants of four polymorphs (α-, β-, γ-, and ε-CL-20) under pressure and temperature are predicted. Our molecular dynamics simulated results of elastic constants of ε-CL-20 at ambient conditions present good agreement with the experimental data. The predicted elastic constants of four polymorphs under pressure and temperature should be accurate and provide powerful guidelines for further experimental measurements. In terms of the Voigt-Reuss-Hill approximation, the mechanical modulus are obtained.

References:

[1] Chen F, Zhou T, Wang Y L, *et al*. Theoretical study on the crystal morphologies of HNBP and PYX [J]. J At Mol Phys(原子与分子物理学报), 2020, 37: 361.

[2] Zhao G Z, Fan J M, Yang D F, *et al*. Molecular design of energetic bicyclo-HMX derivatives: Insights from density functional theory [J]. J At Mol Phys(原子与分子物理学报), 2019, 36: 391.

[3] Pinkerton A A. Private communication [Z]. 1999.

[4] Gump J C, Peiris S M. Phase transitions and isothermal equations of state of epsilon hexanitrohexaazaisowurtzitane (CL-20) [J]. J Appl Phys, 2008, 104: 083509.

[5] Byrd E F C, Rice B M. *Ab initio* study of compressed 1, 3, 5, 7-tetranitro-1, 3, 5, 7-tetraazacyclooctane (HMX), cyclotrimethylenetrinitramine (RDX), 2,4,6,8,10,12-hexanitrohexaazaisowurzitane (CL-20) 2,4,6-trinitro-1,3,5-benzenetriamine (TATB), and pentaerythritol tetranitrate (PETN) [J]. J Phys Chem C, 2007, 111: 2787.

[6] Sorescu D C, Rice B M. Theoretical predictions of energetic molecular crystals at ambient and hydrostatic compression conditions using dispersion corrections to conventional density functionals (DFT-D) [J]. J Phys Chem C, 2010, 114: 6734.

[7] Sorescu D C, Rice B M, Thompson D L. Theoretical studies of the hydrostatic compression of RDX, HMX, HNIW, and PETN crystals [J]. J Chem Phys B, 1999, 103: 6783.

[8] Zhu W, Xiao J J, Zhu W H, *et al*. Molecular dynamics simulations of RDX and RDX-based plastic-bonded explosives [J]. J Hazard Mater, 2009, 164: 1082.

[9] Cui H L, Ji G F, Chen X R, *et al*. Phase transitions and mechanical properties of octahydro-1, 3, 5, 7-tetranitro-1, 3, 5, 7-tetrazocine in different crystal phases by molecular dynamics simulation [J]. J Chem Eng Data, 2010, 55: 3121.

[10] Simpson R L, Urtuew P A, Omellas D. CL-20 performance exceeds that of HMX and its sensitivity is moderate [J]. Propell Explos Pyrotech, 1997, 22: 249.

[11] Bircher H R, Mäder P, Mathieu J. Properties of CL-20 based high explosives [C]. Karlsruhe, Germany: Int Annu Conf ICT, 29th (Energetic Materials), 1998.

[12] Xu X J, Xiao H M, Xiao J J, *et al*. Molecular dynamics simulations for pure ε-CL-20 and ε-CL-20-based PBXs [J]. J Phys Chem B, 2006, 110: 7203.

[13] Xu X J, Xiao J J, Huang H, *et al*. Molecular dynamics simulations on the structures and properties

of ε-CL-20(001)/F_{2314} PBX [J]. J Hazard Mater, 2010, 175: 423.

[14] Stevens L L, Eckhardt C J. The elastic constants and related properties of β-HMX determined by Brillouin scattering [J]. J Chem Phys, 2005, 122: 174701.

[15] Zaug J M. Elastic constants of β-HMX and tantalum, equations of state of supercritical fluids and fluid mixtures and thermal transport determinations [C]//Proceedings of the 11th International Detonation Symposium. Snowmass, CO: [s. n.], 1998: 498.

[16] Sewell T D, Bedrov D, Menikoff R, *et al*. Elastic properties of HMX [C]// Furnish M D, Thadhani N N, Horie Y. Shock Compression of Condensed Matter. New York: American Institute of Physics, 2002: 399.

[17] Haussühl S. Elastic and thermoelastic properties of selected organic crystals: acenaphthene, trans-azobenzene, benzophenone, tolane, trans-stilbene, dibenzyl, diphenyl sulfone, 2, 2′-biphenol, urea, melamine, hexogen, succinimide, pentaerythritol, urotropine, malonic acid, dimethyl malonic acid, maleic acid, hippuric acid, aluminium acetylacetonate, iron acetylacetonate, and tetraphenyl silicon [J]. Z Kristallogr, 2001, 216: 339.

[18] Schwarz R B, Hooks D E, Dick J J, *et al*. Resonant ultrasound spectroscopy measurement of the elastic constants of cyclotrimethylene trinitramine [J]. J Appl Phys, 2005, 98: 056106.

[19] Haycraft J J, Stevens L L, Eckhardt C J. The elastic constants and related properties of the energetic material cyclotrimethylene trinitramine (RDX) determined by Brillouin scattering [J]. J Chem Phys, 2006, 124: 024712.

[20] Haycraft J J. The elastic constants and related properties of the epsilon polymorph of the energetic material CL-20 determined by Brillouin scattering [J]. J Chem Phys, 2009, 131: 214501.

[21] Sun H. An ab initio force-field optimized for condensed-phase applications overview with details on alkane and benzene compounds [J]. J Phys Chem B, 1998, 102: 7338.

[22] Andersen H C. Molecular dynamics simulations at constant pressure and/or temperature [J]. J Chem Phys, 1980, 72: 2384.

[23] Berendsen H J C, Postma J P M, Gunsteren W F, *et al*. Molecular dynamics with coupling to an external bath [J]. J Chem Phys, 1984, 81: 3684.

[24] Ewald P P. Evaluation of optical and electrostatic lattice potentials [J]. Ann Phys: New York, 1921, 64: 253.

[25] Watt J P. Hashin-Shtrikman bounds on the effective elastic moduli of polycrystals with monoclinic symmetry [J]. J Appl Phys, 1980, 51: 1520.

[26] Watt J P. Hashin-Shtrikman bounds on the effective elastic moduli of polycrystals with orthorhombic symmetry [J]. J Appl Phys, 1980, 50: 6290.

[27] Voigt W. Lehrburch der Kristallphysik [M]. Leipzig/Berlin: Teubner, 1928.

[28] Reuss A. Berechnung der fließgrenze von mischkristallen auf grund der plastizitätsbedingung für einkristalle [J]. J Appl Math Mech Z Angew Math Mech, 1929, 9: 49.

[29] Hill R. Theelastic behaviour of a crystalline aggregate [J]. Proc Phys Soc A, 1952, 65: 349.

[30] Bolotina N B, Hardie M J, Speer Jr R L, *et al*. Energetic materials: variable-temperature crystal structures of γ- and ε-HNIW polymorphs [J]. J Appl Crystallogr, 2004, 37: 808.

[31] Jacob G, Toupet L, Ricard L, *et al*. Private communication [Z]. 1999.

[32] Murnaghan F D. Finite deformations of an elastic solid [J]. Am J Math, 1937, 49: 235.

[33] Birch F. Finite elastic strain of cubic crystals [J]. Phys Rev, 1947, 71: 809.

引用本文格式:

中　文: 谭嘉进, 李小燕, 于白茹, 等. 高温高压下 CL-20 的晶格参数和力学性能理论模拟[J]. 四川大学学报: 自然科学版, 2021, 58: 014003.

英　文: Tan J J, Li X Yan, Yu B R, *et al*. Theoretical predictions of lattice parameters and mechanical properties of CL-20 under the temperature and pressure [J]. J Sichuan Univ: Nat Sci Ed, 2021, 58: 014003.